Numerical investigation of flow features and acoustic radiation around a round cavity

O. Marsden*, C. Bogey†, C. Bailly‡

Laboratoire de Mécanique des Fluides et d'Acoustique

Ecole Centrale de Lyon & UMR CNRS 5509

36 avenue Guy de Collongue, 69134 Ecully cedex, France

Acoustic radiation by a circular cylindrical cavity of 10 cm depth and diameter under subsonic turbulent grazing flow is studied experimentally and numerically for free-stream flow velocities of 70, 90 and 110 m/s. Computations are based on the high-accuracy resolution of the full Navier-Stokes equations, allowing the direct computation of the time-dependent sound field in and around the cavity. Computations are performed to scale, and a turbulent upstream boundary layer is generated, in order to match conditions for available experimental data as closely as possible. A description of the flow field inside the cavity is given, and acoustic spectra outside the cavity are compared to available experimental data. Numerical spectra are found to be in good agreement with experimental data, both in terms of predicted frequencies and in terms of amplitudes. The origin of the tonal acoustic emission of the cavity is attributed to a coupling of shear layer dynamics with an acoustic depth mode in the cavity. A model proposed by Elder based on this hypothesis is discussed, and shown to give accurate predictions of discrete frequencies as a function of flow speed.

I. Introduction

The noise generated by civil aircraft both in taking-off and landing phases is currently one of the main aspects limiting traffic growth in large international airports. Among the different causes of total aircraft noise, acoustic radiation due to various elements of the airframe is one of the major sources of total community-perceived aircraft noise during the approach configuration.[1] There are many contributors to total airframe noise, including for example landing gear and high-lift devices, both of which have been the focus of numerous research works. Tonal noise generated by circular burst-disk cavities and vent holes located under wings has received less attention, despite being clearly identifiable[2] even if there is no direct impact on certification levels.

Noise generated by rectangular cavities excited by a grazing flow is a well-researched topic in aeroacoustics and technical reviews are available by Rockwell & Naudascher[3] or Rockwell[4] for instance.

Cavities of cylindrical shape have received far less attention from the research community than their rectangular counterparts. Deep cylindrical cavities, such as organ pipes and cavities encountered in hydraulic side-branches, are an exception. Powell[5] first suggested that organ pipe sound production could be due to an edgetone excitation mechanism interacting with a depth-mode resonance.

*Assistant professor, Ecole centrale de Lyon, email: olivier.marsden@ec-lyon.fr

†CNRS research scientist, Ecole centrale de Lyon

‡Professor at ECL & Institut Universitaire de France

Later researchers developed the idea in more detail, in particular explaining how the resulting pipe frequency was relatively independent from the jet excitation velocity.[6,7] Side branch pipes in hydraulic systems, exhibiting fluid-resonant behaviour, have also been studied in detail.[3] Work has been performed on various aspects such as the flow velocity required for onset of oscillations,[8–10] non-linear coupling of acoustic modes,[11] and the effect of pipe and branch geometry.[12] However, documentation on shallower cylindrical cavities, with a diameter-to-depth ratio of the order of one, is relatively scarce, and limited essentially to work done by Elder,[13] Parthasarathy,[14] Hiwada[15] and more recently Haigermoser and co-workers.[16]
Recently, cylindrical cavities have been enjoying renewed interest from a number of research teams working with numerical simulations to study both flow dynamics and acoustics of such configurations.[17–20] Accordingly, an experimental campaign[18] was recently conducted with the aim of providing reference data to which computations could be compared for a free-stream velocity ranging from 70 to 110 m/s. Acoustic tones dependent on both cavity depth and flow velocity were observed. An illustration of the velocity dependence for a cavity of both depth and diameter equal to 10 cm is proposed in Figure 1, which shows a frequency-velocity PSD plot on the left and the PSD at 1 m above the cavity for flow velocities of 70, 90 and 110 m/s on the right.
The present work attempts to provide preliminary additional details regarding the flow physics and coupling mechanisms at play for this cavity flow problem, by the study of computations performed for the three velocities represented in Figure 1 (right).

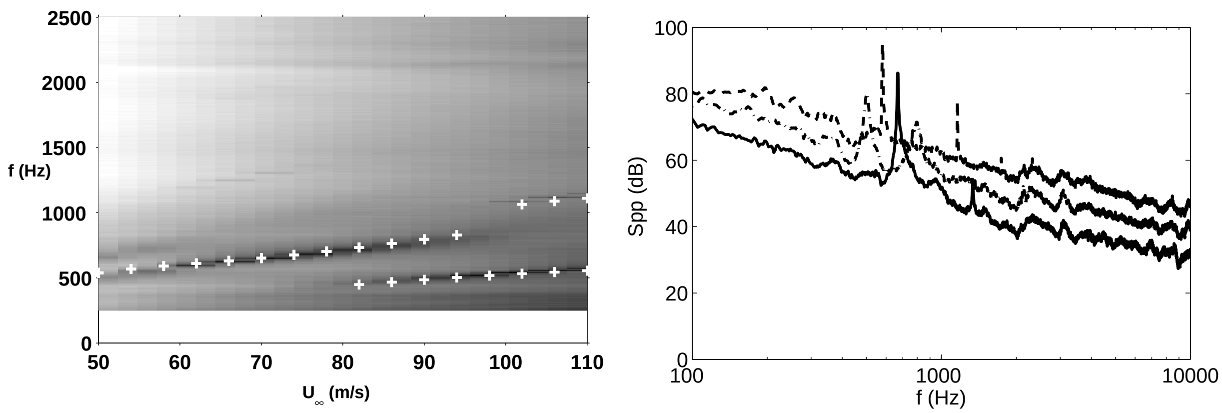

Figure 1. Experimental PSD at 1 m above the cavity as a function of free-stream velocity, for a cylindrical cavity of depth and diameter 10 cm. Grey scale from 30 dB (white) to 100 dB (black). More details available in.[18] White crosses correspond to predicted frequencies, see discussion in section V. Experimental PSD for ——— 70, −·−·− 90 and − − − 110 m/s.

In this paper, computational results are first compared with published experimental data.[18] It is found that the computations yield accurate descriptions of flow and acoustic features generated by the cylindrical cavity. A model proposed by Elder[13] describing the coupling between shear layer oscillations and cavity depth modes and developed for a different geometrical configuration is then shown to provide reasonable predictions of acoustic far-field frequencies observed in experiments.

II. Computational parameters and configuration details

Simulations are performed by solving the unsteady compressible Navier-Stokes equations using low-dispersion and low-dissipation finite-difference schemes.[21] A multi-block approach is followed, with cylindrical coordinates being used to represent the circular cavity wall, and Cartesian coordinates for both the centre of the cavity and the outer flow zone. Code parallelisation is based on MPI, and where necessary, inter-grid communication is carried out via optimized interpolation.[22] The

LES approach, referred to as LES-RF for *relaxation filtering*,[23] is based on the explicit application of a low-pass high-order filtering operation to the flow variables, in order to take into account the dissipative effects of the subgrid scales by relaxing turbulent energy only through the smallest discretized scales. It has been implemented with success in previous simulations of subsonic round jets,[23,24] airfoils[25] and cavities.[18,26] Near boundaries, and in particular near solid walls, optimized non-centred finite-difference schemes and filters are used.[27] In order to allow the direct computation of the noise field created by the flow, non-reflecting boundary conditions[28] are prescribed at free boundaries.

Figure 2 provides a sketch of the computational domain as described below. The origin of the coordinate system is located in the centre of the cavity's upper opening. The outer computational domain covers the range $-0.36 < x < 0.52$, $-0.33 < y < 0.33$ and $0 < z < 0.48$, where extents are given in metres, and is discretized by $427 \times 270 \times 102$ points in the streamwise x, cross-stream y and vertical z directions respectively. The cavity walls are meshed by a cylindrical grid composed of $300 \times 30 \times 148$ points in the azimuthal, radial and vertical directions, and the centre is meshed by a Cartesian grid with the same grid spacing as that used in the outer zone. The computations have been performed on an SGI cluster built from 48 Intel Nehalem cores clocked at 2.67GHz, and linked by a QDR Infiniband network. During production runs, an aggregate computational speed of 125 GFlops is obtained.

The upstream flow velocities studied here are 70, 90 and 110 m/s, and an identical boundary layer thickness of 17 mm is chosen, in order to match experimental conditions[18] as closely as possible. A turbulent mean profile based on the single equation model of Guarini[29] is imposed at the entry, and discretized by 30 grid points in the z direction. Slightly downstream of the entry plane at $x = -0.32$, volumetric force terms are injected in order to generate turbulent-like fluctuations in the boundary layer before it reaches the cavity. The injected terms correspond to 7% of the free-stream velocity. The free-stream velocity and diameter-based Reynolds numbers for these cavity flows are in the range $\mathrm{Re_D} = 4.7 \times 10^5$ to $\mathrm{Re_D} = 7.3 \times 10^5$. The 70 ms/ and 110 m/s cases were run for a total of around 400,000 time steps corresponding to about 0.25 s or 110 cavity flyover times, while the 90 m/s case was run for a total of 800,00 time steps or 0.5 s and 220 flyover times. In what follows, flow components are noted U, V and W for the mean values of the velocity field in the x, y and z directions respectively, and u, v and w for the corresponding instantaneous values.

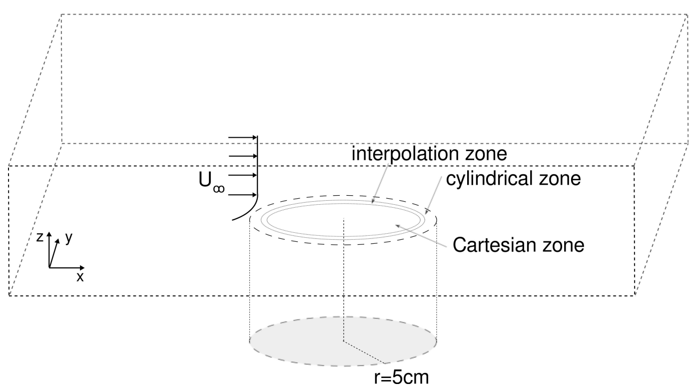

Figure 2. Sketch (not to scale) of the computational domain.

III. Flow in and around the cavity

Computational results are first analzyed in terms of mean flow in and around the cavity.

For the three incoming flow velocities studied in this work, the disturbances injected into the boundary layer at $x = -0.32$ provide an rms turbulence level just upstream of the cavity edge of around 15% of free-stream velocity. These levels are larger than those observed experimentally, but are deemed to show a satisfactory agreement given the focus of the current study.

Computational results show that inside the cavity, mean flow for all three flow velocities is mainly constituted by a single large recirculation vortex whose axis of rotation is aligned with the y direction. Figure 3 illustrates this by showing the streamwise component of the average velocity field in the $y = 0$ plane in black lines, as well as a vector plot of the local mean flow direction in this plane. Both the line plots of U and the vector plot of (U, W) are non-dimensionalized, by the free-stream velocity for the line plots, and by the maximum velocity inside the cavity for the vector plot. The main recirculation is noticeable for the three flow velocities, with a roughly elliptical shape whose long axis is tilted by about 45^o clockwise from the vertical z axis. The centre of the recirculation zone is located around $x = -0.015$ m and $z = -0.08$ m. The mean recirculation velocity is observed to be substantially stronger along the downstream and bottom walls than up the upstream upstream wall. While the general shape of the mean velocity field is not strongly affected by the variation in U_∞, the strength of the recirculation clearly is. Indeed, the ratio of maximum downwards flow to free-stream velocity increases from 33% for $U_\infty = 70$ m/s to 42% for $U_\infty = 110$ m/s.

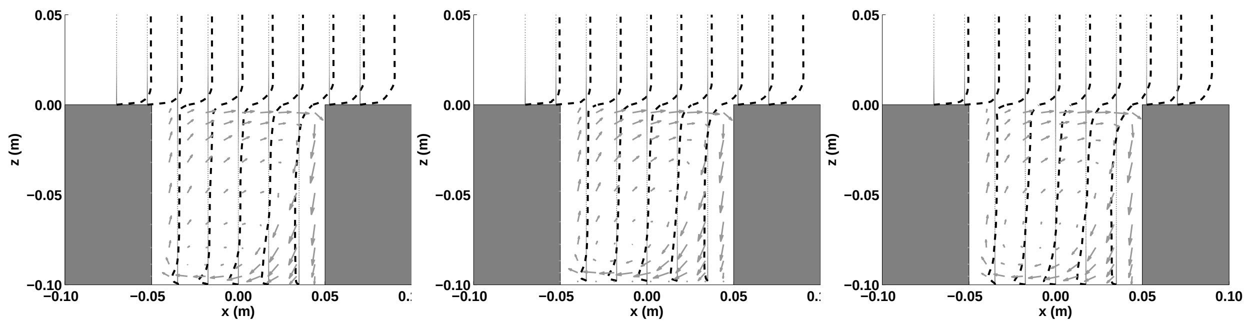

Figure 3. Non-dimensionalized mean streamwise U/U_∞ velocity profiles, in black lines, and vector plot of $(U, W)/max(\sqrt{U^2 + W^2})$, as grey arrows. Free-stream flow velocities of 70 m/s (left), 90 m/s (middle) and 110 m/s (right).

A similar representation of the cross-stream V average velocity component inside the cavity on the $x = 0$ plane, as well as a vector plot of the average (V, W) field in the plane, is illustrated in Figure 4.

An interesting two-tier structure is observed, with a first pair of counter-rotating vortices located at a height of $z = -0.04$ m and a second pair at $z = -0.085$ m.

The effect of increasing free-stream velocity is more marked on the cross-stream flow component than on the streamwise component shown in Figure 3. The ratio of the vertical W component to the free-stream velocity increases from 11% for $U_\infty = 70$ m/s to 16% for $U_\infty = 110$ m/s, and for the cross-stream V component the ratio increases from 17.9% to 29.6%, and the shape of the recirculation is also slightly affected.

Static pressure distribution on the cavity wall can give useful insight into the behaviour of the mean flow, and in particular its differences with respect to a more typical rectangular cavity flow. Moreover experimental data is available for the free-stream velocity of $U_\infty = 70$ m/s, see for example.[18] Figure 5 represents the pressure coefficient C_p on the cavity wall for the three flow velocities of interest. These pressure plots confirm that the flow field inside the cavity is symmetrical for the three velocities studied here. For smaller depth-to-diameter ratios of around 0.5, it has been shown that a strongly asymmetric mean flow can be generated[15,30,31] but such phenomena have not been observed for a depth-to-diameter ratio of one, as in this work. The plot at 70 m/s is in

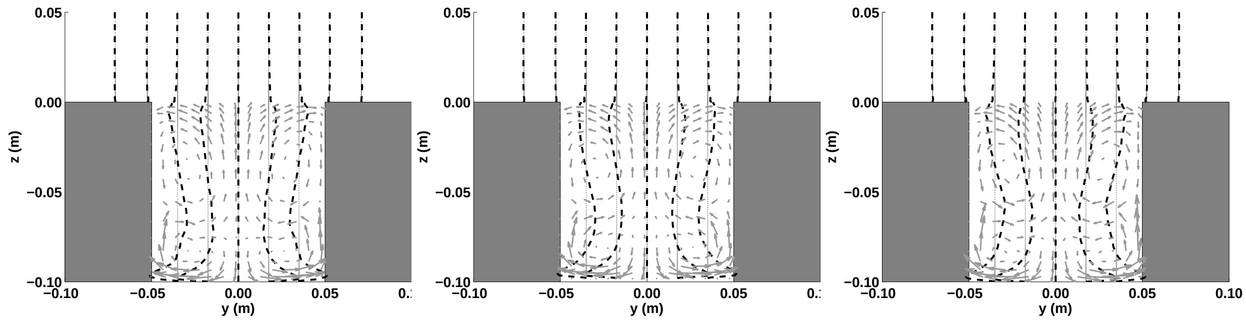

Figure 4. Non-dimensionalized mean cross-stream $V/\max(V)$ velocity profiles, in black lines, and vector plot of $(V,W)/\max(\sqrt{V^2+W^2})$, as grey arrows. Free-stream flow velocities of 70 m/s (left), 90 m/s (middle) and 110 m/s (right).

good quantitative agreement with experimental data obtained for the same configuration.[18] On the C_p plots, the trace of the aforementioned large central recirculation zone, rotating around an axis aligned with the cross-flow direction, can be located thanks to the strong negative C_p zones centred around $\theta = \pm 90^o$ and $z = -0.05$ m. The impact zone of the shear layer on the downstream wall is clearly visible, corresponding to the zone of positive C_p centred around $\theta = 0$ near $z = 0$. Its maximum ranges from 0.18 for $U_\infty = 70$ m/s to 0.23 for $U_\infty = 110$ m/s. This is substantially lower than for rectangular cavities for similar length-to-depth ratios and Mach numbers, where the C_p in the impact zone is typically around 0.3-0.4. In the downstream bottom corner, there is a small counter-rotating recirculation, visible by its positive C_p, which is just observable in the vector plots of Figure 3. The effect of U_∞ on the recirculation is again visible, the recirculation's increasing strength explaining the larger values of C_p observed over the whole cavity wall.

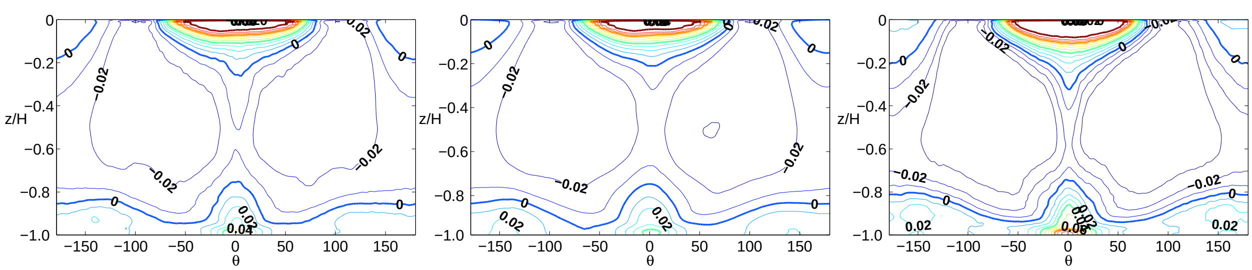

Figure 5. Mean pressure coefficient C_p on the cavity wall as a function of the polar angle θ, where $\theta = 0^o$ designates the downstream direction. Free-stream flow velocities of 70 m/s (left), 90 m/s (middle) and 110 m/s (right). Colour scale from -0.04 to 0.25.

Instantaneous snapshots of the streamwise u velocity and the magnitude of the ω_y component of the vorticity are provided in Figure 6. Of note on these illustrations are the two large-scale structures visible in the velocity and vorticity fields at 70 m/s, and the single large-scale structure apparent at 110 m/s. At 90 m/s, it is harder to discern a characteristic vortical structure in the snapshot.

IV. Acoustic results

It is well known that deep cylindrical cavities exhibit a strong acoustic resonance at their quarter-wavelength frequency. The resonant frequency of interest for a cavity of depth h is given by $f_c = c_0/4(h + \delta_h)$ where $\delta_h = 0.8216 \times r$ corresponds to the acoustic correction length for an

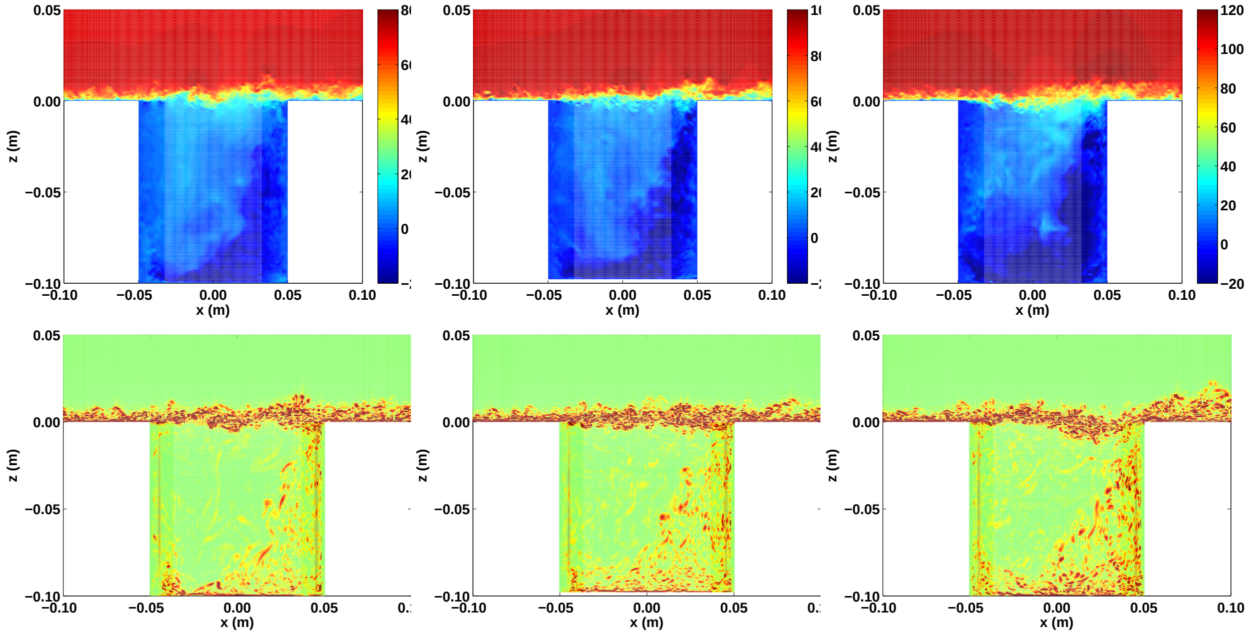

Figure 6. Top: snapshots of u velocity field in the $y = 0$ plane of the cavity. Bottom: snapshots of the magnitude of the ω_y component of vorticity. Colour scale from 0 to $200 \times U_\infty$. Free-stream flow velocities of 70 m/s (left), 90 m/s (middle) and 110 m/s (right).

infinitely flanged open pipe of radius r.[32] For the present cavity depth of 10 cm, this leads to a frequency of $f_c \simeq 607$ Hz. It should be noted however that the aspect ratio $2r/h$ is equal in this case to one, and in that respect the cavity should not be qualified as deep.

In the present configuration, where the cavity is excited by a grazing flow, the far-field acoustic PSD has maxima that vary strongly with flow velocity, as shown in the left-hand side of Figure 1, extracted from experimental work on the same configuration.[18] Such behaviour is reminiscent of that observed for rectangular cavities, see similar plots for example in,[33] and is often attributed to a Rossiter-like coupling across the cavity opening. Experimental results indicate however that the PSD maxima are also strongly depth-dependent, their frequency decreasing as cavity depth is increased.[18] Thus a feedback mechanism based only on the free-stream velocity and on the cavity mouth length is not sufficient to describe the tonal acoustic radiation observed for the cavity configuration of interest.

The acoustic field at 1 m above the cavity, represented as a power spectral density, is plotted in Figure 7, in solid black lines for experimental results, and in dash-dotted blue lines for computational data, for the three free-stream velocities of interest. Experimental spectra are computed from signals recorded at a sampling frequency of 25 kHz, by averaging 100 periodgram estimates of the PSD based on 8192 sample points. The PSD are thus represented with a Δf of 3 Hz. Numerical spectra are computed in a similar fashion but from much shorter time signals, of varying lengths depending on the free-stream velocity, and as a result have a slightly higher Δf of 6 Hz.

For each free-stream velocity, the experimental results are first described, before analyzing the computational spectra. At 70 m/s, a single acoustic peak is found at a frequency of 660 Hz, about 10% above the acoustic depth resonance frequency, emerging from the broadband noise by around 27 dB to reach 87 dB. Its first harmonic is also distinctly visible, at a frequency of 1320 Hz. The computation reproduces the main lower frequency peak reasonably well. The shape and frequency of the peak are well matched, however its amplitude is underpredicted by around 7 dB. The first harmonic is not visible in the computational PSD. This harmonic is not a natural cavity depth mode, which suggests that its origin is of a non-linear nature, see the discussion in the next section. Thus the numerical underprediction of the fundamental frequency might explain the absence of the first harmonic in the computation. Above the frequency of the main peak, the broadband noise level is correctly captured by the computation. For lower frequencies, broadband noise is substantially underpredicted, which is to be expected for computational PSDs. There are nevertheless strong subharmonics present in the signal, which translate to a burst-like structure for the computed pressure time signal. Neither the origin of this phenomenon nor its physical relevance have as yet been ascertained.

The 90 m/s configuration yields an acoustic field with two distinct peaks, the first at a frequency of 500 Hz and the second at a frequency of 795 Hz. The lower frequency peak is slightly more intense, reaching a maximum of 80 dB, while the the higher frequency peak reaches 72 dB. Neither of the two peaks exhibits discernable harmonics. The computation captures the presence of the two peaks, but their amplitudes are too low, by around 8 and 7 dB respectively. The frequency of the lower peak is also overpredicted by approximately 30 Hz. Once again the higher frequency broadband level is very well matched and the lower frequency range underestimated, but in this case there is no noticeable low frequency modulation in the pressure signal, as was observed for the 70 m/s computation.

Finally the 110 m/s flow velocity results in a single intense acoustic peak at a frequency of 580 Hz. The peak has a considerably higher quality factor than that observed at 70 m/s, and emerges from the background noise by more than 30 dB to reach a maximum of 96 dB. Its first harmonic at 1180 Hz is also very pronounced, with an emergence of 18 dB, and in fact the second and third harmonics are noticeable in the experimental PSD. The numerical PSD reproduces the fundamental and its harmonic well, with a slight overprediction of the frequency by around 15 Hz. The fundamental's level is marginally overestimated, while its first harmonic is slightly too low. Broadband noise trends are similar to those observed for the two previous cases.

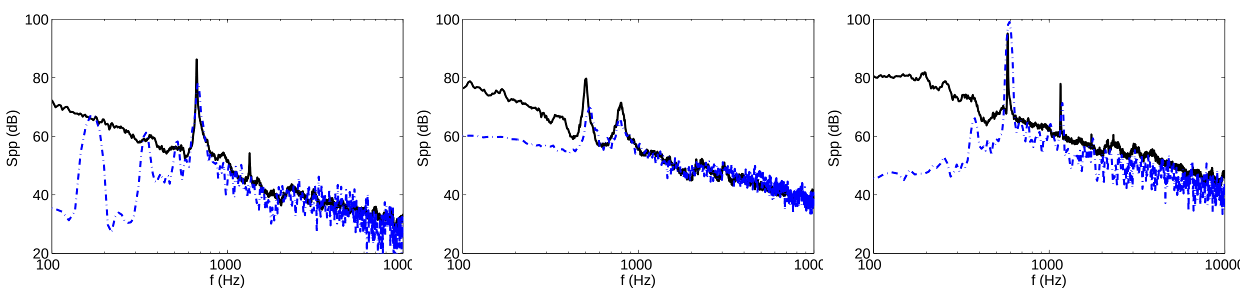

Figure 7. Acoustic PSD (Pa^2/Hz) at $(x, y, z) = (0, 0, 1)$, 1 m above the cavity: — experiment, – · – computation, for $U_\infty = 70$ m/s (left), 90 m/s (middle) and 110 m/s (right).

V. Discussion

The origin of the far-field cavity tones is now discussed. Working on somewhat similar configurations, Elder[13] and Parthasarathy[14] both came to the conclusion that tonal acoustic radiation was due to coupling between a cavity depth mode and the shear layer dynamics. Elder also proposed a physical model that yielded good frequency predictions for his study, namely that of tones generated by a deep cylindrical cavity grazed by low-subsonic flow and partially closed by a rectangular mouth. His model is based on the assumptions that the shear layer development is forced by the acoustic depth mode standing wave formed inside the cavity, and that the fluctuating mass flow into and out of the cavity is responsible for maintaining the standing wave's amplitude, as described in depth for the case of organ pipes.[7] According to this approach, stable acoustic tones should thus occur at frequencies such that the product of the forward transfer function, giving mass flow as a function of acoustic forcing, by the backward transfer function, describing acoustic forcing resulting from a given fluctuating mass flow, is equal to one.

Preliminary comparisons between predictions from Elder's model and experimental and computational results used in this study are presented. A brief summary of Elder's model as he applied it to his work is provided in what follows; its derivation is however not presented in detail here, as it is not the object of this work. Interested readers are referred to sections I and II of Elder's paper[13] for illustrations and an in-depth discussion. The aforementioned backward transfer function G_{21} is written assuming that the driving flow sees the cavity as a parallel resonant circuit. Using Elder's notations, where $q_M = u_M S$ is acoustic volume flow through the cavity opening of section S and q_J the fluctuating volume flow into and out of the cavity due to shear layer displacement, we can write $G_{21} = -Z_C/(Z_M + Z_C)$ where Z_C is the cavity impedance looking in from the mouth, and Z_M the mouth impedance looking out from inside the cavity. For the forward transfer function, Elder estimated the fluctuating mass flow from the time-dependent displacement of the shear layer, which in turn was modeled via linear stability theory. The displacement of the interface is assumed to be independent of the cross-stream y coordinate, and can therefore be written as $\xi(x,t) = A\cos(\omega t + \phi)$. This term can be decomposed as the sum of the displacement resulting from the acoustic velocity generated by the cavity, $(u_M/i\omega)e^{i\omega t}$, and the transverse wave term predicted by linear stability theory, $Ae^{\alpha x}e^{i(\omega t - kx)}$. Drive flow is then expressed as $q_J = bU_o\xi_M$, where b is the slot width in the spanwise direction, ξ_M the maximum interface displacement, and U_o the average flow velocity for $z = 0$ at the streamwise position of maximum interface displacement. Finally, the FTF G_{12} can be written as $G_{12} = (U_o/H\omega)e^{-i(kH-\pi)}$ where H is the slot opening length in the streamwise direction. The wavenumber k is obtained from linear stability theory[34] as a function of frequency f, free-stream flow velocity U_∞ and an upstream length scale of the initial shear layer $U_\infty/(2dU/dz)$. Stationary harmonic oscillating states, or in other words states yielding a tonal acoustic field, should then verify the condition $G_{12}G_{21} = 1$.

Elder used this condition to obtain oscillation parameters at resonance, *i.e.* at frequencies corresponding exactly to a cavity depth mode, and to determine for what slot lengths H resonance would be achieved. In the present work, the approach is used to estimate the effect of flow velocity on acoustic frequencies emitted by a round cavity. It should be noted that no slot or aperture is present at the cavity opening, and thus the equivalent streamwise mouth length, referred to as H by Elder, is now dependent on the cross stream y coordinate and equal to $2\sqrt{r^2 - y^2}$. It is therefore no longer natural to assume that the phase of the interface displacement be constant in the spanwise direction; in what follows, the model is applied to a zone along the streamwise diameter of the cavity opening for which the previous assumption can reasonably be made. Other notable differences with Elder's experimental configuration include the much smaller depth-to-diameter ratio of around one in this work, and flow velocities higher by a factor of two to four. The cavity impedance formulation is unchanged, but the linear mouth impedance is now known theoretically, from the work of Nomura *et al.*[32] for an infinitely flanged pipe. The influence of grazing flow on the termination impedance depends strongly on the ratio of diameter to boundary layer thickness, a subject not discussed by Elder. For small diameters, typically $d_0/\delta < 0.5$, numerous studies focused on acoustic liner behaviour have shown that resistance increases roughly linearly with grazing flow speed,[35,36] while reactance varies in a less predictable fashion. For larger orifices also, impedance varies with grazing flow as a function of the diameter-based Strouhal number, as measured by Ronnenberger.[37] However, given the high minimum Strouhal number of oscillations observed in this work, $St_{min} = \omega d_0/U_\infty = 2\pi \times 580 \times 5\ 10^{-2}/110 = 1.66$, the cavity mouth impedance should not vary significantly from its value in the absence of grazing flow. Therefore, a mouth impedance of $Z_M = (\rho c/S)(r_L + ik_0\delta h) =$ is used, where $\delta h = 0.8216\, r_0$ and $r_L = 1/2\ (k_0 r_0)^2$.[32] Unlike in Elder's work, in this study it is not necessary to add a non-linear resistance term $|u_M|/c_0$

in the mouth impedance, as the small depth-to-diameter ratio induces large linear resistance in the mouth: $|u_M|/c_0 << 1/2(k_0 r_0)^2$. The complex backward and forward transfer functions as described above should yield a product of $G_{12} \times G_{21} = 1$ at frequencies where stationary acoustic radiation is observed.

The physical significance of the previous condition can be made clearer by splitting the relation into its real and imaginary parts. The imaginary part, $\mathrm{Im}(G_{12}G_{21}) = 0$, describes a phase relation which must be met for oscillations to be stationary; it is the analogue for this configuration of the frequency relation proposed by Rossiter for rectangular cavities. The real part, $\mathrm{Re}(G_{12}G_{21}) = 1$, simply states that for cavity oscillation to be stable in time, the acoustic energy lost during each cycle due to attenuation in the cavity and radiation through the mouth must be exactly compensated by the energy supplied by the drive flow, *i.e.* the fluctuating shear layer. With parameter values relevant to this study, the imaginary part of the condition $\mathrm{Im}(G_{12}G_{21}) = 0$ is met for certain velocity-dependent frequencies. As noted by Elder, these frequencies approximately verify the condition $kd_0 = 2\pi m - \pi/2$, where $m = 1, 2, 3, \ldots$ corresponds to the number of large-scale vorticies in the shear layer. The first two modes predicted by $\mathrm{Im}(G_{12}G_{21}) = 0$, as well as the harmonics of the mode (m=1), are shown in Figure 1 (left) by white crosses. A good agreement is observed for both modes at all frequencies. This strongly suggests that the dominant behaviour for this configuration is the acoustic depth mode coupling with the two first shear layer modes. According to this hypothesis, the 70 m/s flow velocity should be marked by two vortical structures on average across the cavity diameter, and the 110 m/s case by a single structure. This point can be confirmed by examples of phase-averaged computational velocity fields at 70 m/s and 110 m/s, shown in Figure 8. These illustrations were obtained by averaging the vertical w component of the velocity fields with respect to the phase of a far field pressure signal. A total of 16 phase bins was used for each case, and each bin contained around 100 velocity fields. This simple treatment clearly shows as anticipated the two structures for the lower velocity and one single large structure for the higher velocity, a structure here referring to a zone of positive velocity followed by a zone of negative velocity.

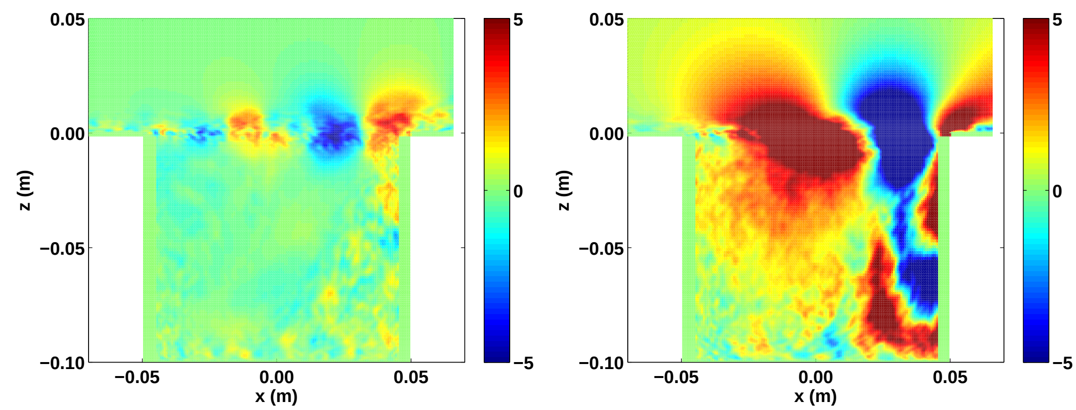

Figure 8. Phase-averaged $\tilde{w}$ velocity fields in m/s obtained from computations at 70 m/s (left) and 110 m/s (right).

However, the real part of the transfer function product, $\mathrm{Re}(G_{12}G_{21})$, is substantially too small, and the overall condition is not met over frequency range studied in this work. The reason for the strong disparity in the magnitude of the transfer function product $G_{12}G_{21}$ appears to lie in the amplitude of the G_{12} function. In Elder's work, this amplitude is determined from the maximum amplitude of the shear interface displacement ξ_M, which for him was well matched by the acoustic displacement $|u_M/\omega|$. Thus his FTF does not explicitly depend on the shear layer velocity profile. Elder explained this amplitude term with the observation that the convective growth term α for linear instabilities was "quenched" a few millimeters downstream of the leading edge, leading to an interface fluctuation amplitude independent of the streamwise position x. For the configurations of interest here, the situation is quite different, with experimental results showing a growth of ξ over the whole cavity diameter, and also with the driving volume flow q_J appearing not to be well modelled by the expression $q_J = bU_o\xi_M$ where b for the cylindrical cavity would be roughly $2\sqrt{r_0^2 - (\lambda/4)^2}$.

In order to illustrate the first point, approximate particle emission lines, or interface waves, are shown at four equally spaced times in the acoustic period in Figure 9 for a free-stream flow velocity of 70 m/s. These interface waves have been inferred from high-speed shear layer PIV images as follows. The PIV flow fields are sorted and phase-averaged with respect to a pressure signal recorded at the bottom of the cavity, which is synchronized with the PIV system. The pressure signal shows a strong harmonic peak, but nevertheless also exhibits long periods during which the main frequency is drowned out by other flow features. Only images corresponding to relatively sinusoidal portions of the pressure signal are retained for the phase averaging. In practice about half of the signal was rejected based on this criterion. The remaining flow fields are separated into twelve time intervals or bins, and each bin is averaged according to the technique proposed by Hussain and Reynolds[38] to obtain the ensemble averaged and cyclic vertical components of the shear layer W and $\tilde{w}$. The phase-averaged fields thus obtained are used to compute particle emission lines from the upstream cavity edge. These time-dependent emission lines are represented by dashes in Figure 9. Unlike in Elder's case, interface displacement clearly grows as perturbations are convected along the shear layer, and the maximum displacement is roughly five times greater than the acoustic displacement.

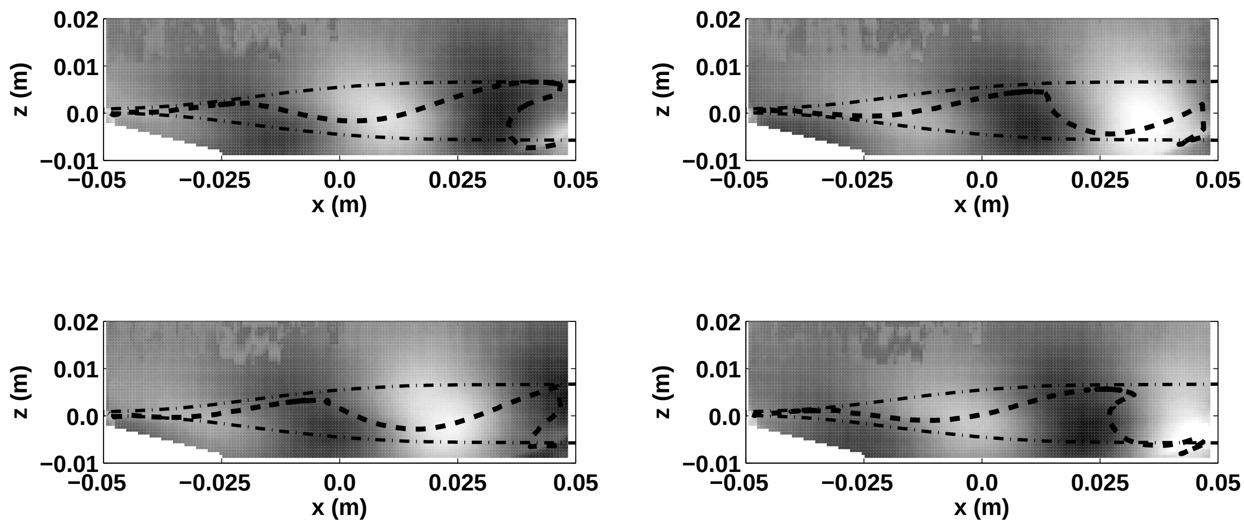

Figure 9. Interface (dashed line) and cyclic vertical velocity perturbations during one acoustic cycle, estimated from high-speed PIV for a free-stream flow velocity of 70 m/s. Grey scale ranges from -6 (white) to 6 (black) m/s. The perturbation envelope predicted by linear stability theory[34] is represented as dashed-dotted lines.

Also represented in Figure 9 is the spatial envelope of fluctuations assuming that the initial acoustic displacement $|u_M/\omega|$ is amplified during its convection across the cavity mouth by the local spatial growth rate predicted by linear stability theory.[34]This envelope is represented by dashed-dotted lines in Figure 9. For a given wavenumber k, the local spatial growth rate α depends on the local velocity profile slope dU/dz, which can be obtained from the PIV data. The consequence of this is unfortunately that the maximum displacement ξ_M used in G_{12} is now a function of $\alpha(x)$ which in turn is a function of dU/dz : $\xi_M = \mathcal{C}\,u_M/\omega$, where $\mathcal{C} \simeq \int_{-r_0}^{r_0-\lambda/4} \alpha(x)dx$. It can be seen from

Figure 9 that the maximum displacement is in fact reasonably well predicted by the envelope.
The second point in question deals with the expression $q_J = bU_o\xi_M$. The PIV flow data allows ξ_M to be estimated at around 6 mm according to the technique described previously, and $U_o =$ 25 m/s. The driving volume flow would thus be $q_J \simeq 1.8 \times 10^{-2} \cos(\omega t)$ m^3/s. Supposing that $\tilde{w}$ is independent of y, the phase-averaged cyclic velocity fluctuation $\tilde{w}(x, z, t)$ can also be used directly to obtain an estimation of q_J according to $q_J(t) = \int_{-r_0}^{r_0} 2\sqrt{r_0^2 - x^2}\tilde{w}(x, z = 0, t)dx$ which yields $q_J(t) \simeq 4 \times 10^{-3} \cos(\omega t)$ m^3/s. The reason for this large difference between these two estimations of q_J is unclear. Nevertheless, with the second estimation obtained by integrating $\tilde{w}(x, z = 0, t)$ for 70 m/s, the product $G_{12}G_{21}$ has a value of 1.1, very close to the expected value of 1. Thus Elder's approach successfully predicts frequencies at which oscillations can be observed for the configurations studied in this work, but predicted thresholds for the appearance and disappearance of these frequencies as a function of flow speed as well as these frequencies' amplitudes, are highly unreliable due to considerable uncertainty in the determination of the forward transfer function's magnitude.
Computations such as those presented in this work provide an useful tool for examining the underlying hypotheses of physcial models like Elder's. A more detailed study of the shear layer dynamics and their relationship to the fluctuating drive flow q_J based on computational data is currently underway.

VI. Concluding remarks

Acoustic radiation by a circular cylindrical cavity of 10 cm depth and diameter under subsonic turbulent grazing flow has been studied both by experiments and by numerical computations. Based on computational results, the structure of the mean flow inside the cavity is described. An accurate numerical prediction of tonal emission and its dependence on free-stream flow velocity is obtained, in terms of both frequency and amplitude.
A physical model developed for a different geometrical configuration is shown to a good estimation of acoustic frequencies emitted by the cavity. Tonal radiation is described in the model by the coupling between the cavity's quarter-wavelnegth depth mode and the dynamics of the grazing shear-layer. Computations provide useful insight into the validity of the model, and confirm that tonal noise is due to coupling between the cavity's acoustic depth mode and shear layer dynamics. Further computations are underway to study in more depth the mechanisms involved in this coupling.

Acknowledgments

This research project is supported by the *Fondation de Recherche pour l'Aéronautique & l'Espace (FRAE)* under the contract reference AFB AEROCAV, and in collaboration with following french laboratories: ONERA, SINUMEF, IUSTI and INRIA. The team was granted access to the HPC resources of the Institut du Développement et des Ressources en Informatique Scientifique (IDRIS) under the allocation 2010-020204 made by GENCI (Grand Equipement National de Calcul Intensif).

References

[1]Hubert, J., "Jet noise assessment and sensitivity at aircraft level," *AIAA Paper 2007-3728*, 2007, pp. 1–11.

[2]Czech, M., Crouch, J., and Stoker, R., "Cavity noise generation for circular and rectangular vent holes," *AIAA Paper 2006-2508*, 2006.

[3]Rockwell, D. and Naudascher, E., "Review - Self-sustaining oscillations of flow past cavities," *ASME Journal of Fluids Engineering*, Vol. 100, 1978, pp. 152–165.

[4]Rockwell, D., "Oscillations of impinging shear layers," *AIAA Journal*, Vol. 21, No. 5, 1983, pp. 645–664.

[5]Powell, A., "On the edgetone," *J. Acoust. Soc. Am.*, Vol. 33, No. 4, 1961, pp. 395–409.

[6]Cremer, L. and Ising, H., "Die selbsterregte schwingungen von orgelpfeifen," *Acústica*, Vol. 19, 1967, pp. 143–153.

[7]Elder, S., "On the mechanisms of sound production in organ pipes," *J. Acoust. Soc. Am.*, Vol. 54, No. 6, 1973, pp. 1554–1564.

[8]Howe, M., "The dissipation of sound at an edge," *Journal of Sound and Vibration*, Vol. 70, No. 3, 1980, pp. 407–411.

[9]Bruggeman, J., *Flow-induced pulsations in pipe systems*, Phd. thesis, Eindhoven University of Technology, 1987.

[10]Ziada, S. and Shine, S., "Strouhal numbers of flow-excited acoustic resonance of closed side branches," *J. Fluids Struct.*, 1999.

[11]Ingard, U. and Singhal, V., "Flow excitation and coupling of acoustic modes of a side-branch gravity in a duct," *J. Acoust. Soc. Am.*, Vol. 60, No. 5, 1976.

[12]Jungowski, W., Botros, K., and Studzinski, W., "Cylindrical side-branch as tone generator," *Journal of Sound and Vibration*, Vol. 131, No. 2, 1989, pp. 265–285.

[13]Elder, S., "Self-excited depth-mode resonance for a wall-mounted cavity in turbulent flow," *J. Acoust. Soc. Am.*, Vol. 64, No. 3, 1978, pp. 877–890.

[14]Parthasarathy, S., Cho, Y., and Back, L., "Sound generation by flow over relatively deep cylindrical cavities," *J. Acoust. Soc. Am.*, Vol. 78, No. 5, 1985, pp. 1785–1795.

[15]Hiwada, M., Kawamura, T., Mabuchi, I., and Kumada, M., "Some characteristics of flow pattern and heat transfer past a circular cylindrical cavity," *Bulletin of the JSME*, Vol. 26, No. 220, October 1983.

[16]Haigermoser, C., Scarano, F., and Onorato, M., "Investigation of the flow in a circular cavity using stereo and tomographic particle image velocimetry," *Experiments in Fluids*, Vol. 46, No. 3, 2009, pp. 517–526.

[17]Hering, T., Dybenko, J., and Savory, E., "Experimental verification of CFD modeling of turbulent flow over circular cavities," *CSME*, 2006.

[18]Marsden, O., Jondeau, E., Souchotte, P., Bailly, C., Bogey, C., and Juvé, D., "Investigation of flow features and acoustic radiation of a round cavity," *AIAA Paper 2008-2851*, 2008.

[19]Mincu, D., Mary, I., and Redonnet, S., "Numerical Simulations of the Unsteady Flow and Radiated Noise Over a Cylindrical Cavity," *AIAA Paper 2008-2917*, 2008.

[20]Mery, F., Mincu, D., and Casalis, G., "Noise Generation Analysis of a Cylindrical Cavity by LES and Global Instability," *AIAA Paper 2009-3205*, 2009.

[21]Bogey, C. and Bailly, C., "A family of low dispersive and low dissipative explicit schemes for noise computations," *Journal of Computational Physics*, Vol. 194, No. 1, 2004, pp. 194–214.

[22]Desvigne, D., Marden, O., Bogey, C., and Bailly, C., "Development of non-centered wavenumber-based optimized interpolation schemes with amplification control for overlapping grids," *Society for Industrial and Applied Mathematics*, 2010, to appear.

[23]Bogey, C. and Bailly, C., "Turbulence and energy budget in a self-preserving round jet: direct evaluation using large-eddy simulation," *Journal of Fluid Mechanics*, Vol. 627, 2009, pp. 129–160.

[24]Bogey, C. and Bailly, C., "Large Eddy Simulations of transitional round jets : influence of the Reynolds number on flow development and energy dissipation," *Physics of Fluids*, Vol. 18, 2006, 065101.

[25]Marsden, O., Bogey, C., and Bailly, C., "Direct Noise Computation of the Turbulent flow around a zero-incidence airfoil," *AIAA Journal*, , No. 4, 2008, pp. 874–883.

[26]Marsden, O., Gloerfelt, X., and Bailly, C., "Direct noise computation of adaptive control applied to a cavity flow," *C. R. Acad. Sci.*, Vol. 331, 2003, pp. 423–429.

[27]Berland, J., Bogey, C., Marsden, O., and Bailly, C., "High-order, low dispersive and low dissipative explicit schemes for multiple-scale and boundary problems," *Journal of Computational Physics*, Vol. 224, 2007, pp. 637–662.

[28]Bogey, C. and Bailly, C., "Three-dimensional non-reflective boundary conditions for acoustic simulations : far field formulation and validation test cases," *Acta Acustica*, Vol. 88, No. 4, 2002, pp. 463–471.

[29]Guarini, S. E., Moser, R. D., Shariff, K., and Wray, A., "Direct numerical simulation of a supersonic turbulent boundary layer at Mach 2.5," *Journal of Fluid Mechanics*, Vol. 414, No. 1, 2000, pp. 1–33.

[30]Dybenko, J. and Savory, E., "An experimental investigation of turbulent boundary layer flow over surface-mounted circular cavities," *CSME Forum*, 2006.

[31]Marden, O., Bogey, C., and Bailly, C., "Numerical investigation of flow features and acoustic radiation from round cavities," *ECCOMAS CFD 2010, Portugal*, 2010.

[32]Nomura, Y., Yamamura, I., and Inawashiro, S., "On the acoustic radiation from a flanged circular pipe," *J. Phys. Soc. Jap.*, Vol. 15, No. 3, 1960.

[33]Malone, J., Debiasi, M., Little, J., and Samimy, M., "Analysis of the spectral relationships of cavity tones in subsonic resonant cavity flows," *Physics of Fluids*, , No. 21, 2009.

[34]Michalke, A., "On spatially growing disturbances in an inviscid shear layer," *Journal of Fluid Mechanics*, Vol. 23, No. 3, 1965, pp. 521–544.

[35]Goldman, A. and Panton, R., "Measurement of the acoustic impedance of an orifice under a turbulent boundary layer," *J. Acoust. Soc. Am.*, Vol. 60, No. 6, 1976, pp. 1397–1404.

[36]Sun, X., Jing, X., Zhang, H., and Shi, Y., "Effect of grazing-bias flow interaction on acoustic impedance of perforated plates," *Journal of Sound and Vibration*, Vol. 254, No. 3, 2002, pp. 557–573.

[37]Ronnenberger, D., "The acoustical impedance of holes in the wall of flow ducts," *Journal of Sound and Vibration*, Vol. 24, No. 1, 1972, pp. 133–150.

[38]Hussain, A. K. M. F. and Reynolds, W. C., "The mechanics of an organized wave in turbulent shear flow," *Journal of Fluid Mechanics Digital Archive*, Vol. 41, No. 02, 1970, pp. 241–258.